Chiromers: Conformation-driven mirror-image supramolecular chirality isomerism identified in a new class of helical rosette nanotubes

ARTICLE *in* NANOSCALE · APRIL 2014

Impact Factor: 7.39 · DOI: 10.1039/c4nr00340c · Source: PubMed

Nanoscale

PAPER

View Article Online
View Journal

Cite this: DOI: 10.1039/c4nr00340c

Chiromers: conformation-driven mirror-image supramolecular chirality isomerism identified in a new class of helical rosette nanotubes†

Usha D. Hemraz,[ab] Mounir El-Bakkari,[ab] Takeshi Yamazaki,[ab] Jae-Young Cho,[b] Rachel L. Beingessner[b] and Hicham Fenniri*[abcd]

Received 18th January 2014
Accepted 15th March 2014

DOI: 10.1039/c4nr00340c

www.rsc.org/nanoscale

Rosette nanotubes are biologically inspired nanostructures, formed through the hierarchical organization of a hybrid DNA base analogue (G∧C), which features hydrogen-bonding arrays of guanine and cytosine. Several twin-G∧C motifs functionalized with chiral moieties, which undergo a self-assembly process under methanolic and aqueous conditions to produce helical rosette nanotubes (RNTs), were synthesized and characterized. The built-in molecular chirality in the twin-G∧C building blocks led to the supramolecular chirality exhibited by the RNTs, as evidenced by the CD activity. Depending on the motifs and environmental conditions, mirror-image supramolecular chirality due to absolute molecular chirality, solvent-induced and structure-dependent supramolecular chirality inversion, and pH-controlled chiroptical switching were observed.

1 Introduction

Chirality is one of nature's most fascinating features, which can manifest both at the molecular and supramolecular levels.[1–10] While molecular chirality originates from the spatial arrangement of atoms, supramolecular chirality arises either from the association of chiral components or through the dissymmetric interaction of achiral building blocks.[11–13] In most cases, supramolecular chirality is templated by the inherent chirality of the monomer or by chiral additives in an achiral environment. There are various examples of supramolecular chirality which are based on chiral scaffolds,[14–16] the 'Sergeants and Soldiers' principle[17–21] and the 'chiral memory' concept.[22–27] Most of these supramolecular systems are built on π–π stacking interactions, host–guest complexes and hydrogen-bonded assemblies. Among these systems, our group emerged with a new class of nanomaterials called *rosette nanotubes* (RNTs),[27–29] which display remarkable chiroptical behavior.

The RNTs are biocompatible architectures formed through self-assembly of a self-complementary guanine–cytosine (G∧C) hybrid module. In solution, these G∧C motifs self-organize into hexameric macrocycles, which then π–π stack to form the nanotubes (Fig. 1). These motifs can be synthesized to feature either one or two G∧C units in order to generate self-assembled rosettes, which are maintained by 18 or 36 hydrogen bonds, respectively. The twin-RNT construct self-assembled from the twin-G∧C motif is substantially more stable (stable in boiling water) and functional group-tolerant compared to the single-base RNT construct when identically functionalized and of

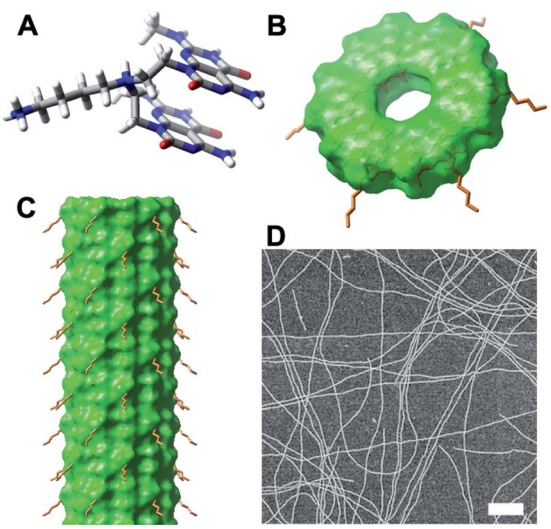

Fig. 1 Model of twin-G∧C motif TBL with an achiral side-chain (A). Hierarchical self-assembly of TBL into double-stacked hexameric rosettes (B) which then further π–π stack to form an achiral RNT (C). SEM image of TBL RNTs (0.017 mM in methanol). Scale bar = 200 nm.

[a]Department of Chemistry, University of Alberta, Edmonton, Alberta, Canada
[b]National Institute for Nanotechnology, 11421 Saskatchewan Drive, T6G 2M9, Edmonton, Alberta, Canada
[c]Department of Chemical and Biomedical Engineering, Northeastern University, 313 Snell Engineering Center, 360 Huntington Avenue, Boston, MA 02115, USA. E-mail: h.fenniri@neu.edu; Fax: +1 6173732209; Tel: +1 6173737690
[d]Biomedical Engineering Research Center, Qatar Biomedical Research Institute, P.O. Box 5825, Doha, Qatar

† Electronic supplementary information (ESI) available. See DOI: 10.1039/c4nr00340c

equal length.[30] Fig. 1 shows an example of an achiral twin-G∧C motif functionalized with butylamine (referred to as TBL). In the absence of a chiral bias, the resulting RNTs, which express these butylamine groups on the outer surface, do not show a preferred helicity (a racemic mixture of P and M helices).[31–33]

In contrast to this, we have also demonstrated several examples of RNTs that exhibit supramolecular chirality. For instance, single G∧C motifs functionalized with amino acids produced helical nanostructures, as evidenced by their circular dichroism (CD) activity.[28] In another example, single G∧C expressing achiral amino-benzo-18-crown-6-ether pendants spontaneously self-assembled to produce a racemic mixture of P and M helical RNTs *via* a dynamic process. Upon binding with chiral amino acids such as L-alanine, only nanotubes of the M-helicity were formed, which was reflected by a characteristic induced CD signal. The L-alanine entrapped within the crown ether created a chiral bias, which upon amplification resulted in the formation of one-handed nanotubes.[27] A new self-assembling tricyclic module, featuring an internal pyridine ring fused with modified guanine and cytosine rings, formed RNTs with increased inner and outer diameters.[34] When functionalized on their outer surface with L-lysine, the RNTs, which exhibit J-type properties, have the largest molar ellipticity ever reported for a chiral helical stack.[35] While these examples deal with single-G∧C motifs, we wanted to explore supramolecular chirality in the twin-RNT system.

Herein, we synthesized several twin-G∧C motifs, which undergo hierarchical self-assembly under methanolic and aqueous conditions to produce RNTs. The built-in molecular chirality in the twin-G∧C building blocks is responsible for the supramolecular chirality exhibited by the RNTs. Depending on the motifs and environmental conditions, the following phenomena were observed: (a) mirror-image supramolecular chirality due to absolute molecular chirality, (b) solvent-induced supramolecular chirality inversion, (c) structure-dependent supramolecular chirality inversion, and (d) pH-induced chiroptical switching.

2 Experimental

2.1 Materials

Compounds R-TBL, S-TBL and K-C4-TBL were prepared according to the synthetic schemes illustrated in Fig. S1–S3,† respectively. K-C2-TBL was synthesized according to a previously reported procedure.[27] K1T–K15T were prepared using solid-phase synthesis techniques (reported elsewhere).[36]

2.2 Self-assembly

Stock solutions of R-TBL, S-TBL, K-C2-TBL and K-C4-TBL were prepared in water or methanol at a concentration of 0.5 mg mL^{-1} and were aged at room temperature. For the K*n*T series, solutions were prepared by dissolving 2 mg of K*n*T in 1 mL of deionized water and allowing the solutions to stand for 1 h. The resulting solutions were then diluted with the appropriate buffers (0.05 M) to produce 1 mg mL^{-1} stock solutions, which were aged for 1 month. Aliquots of these stock solutions were used for microscopy, circular dichroism and UV-vis spectroscopic experiments at different time intervals.

2.3 Circular dichroism

All circular dichroism (CD) spectra were recorded on a JASCO J-810 spectropolarimeter. Samples were scanned from 350 to 205 nm at a rate of 100 nm min^{-1}. The CD spectra of R-TBL, S-TBL, K-C2-TBL and K-C4-TBL were recorded by taking aliquots of the stock solutions and diluting them to 0.025 mg mL^{-1} (3.34×10^{-5} M for R-TBL and S-TBL, and 2.46×10^{-5} M for K-C2-TBL and K-C4-TBL) with deionized water or methanol. For the K*n*T samples, the CD spectra were recorded by taking aliquots of the stock solutions at different pH values and diluting them to 4×10^{-5} M with deionized water.

3 Results and discussion

3.1 Absolute molecular chirality

It is well known that molecules with opposite molecular chiralities produce supramolecular systems with opposite helicities. Twin-G∧C motifs R-TBL and S-TBL (Fig. 2A and B) were synthesized according to the synthetic schemes in Fig. S1 and S2.† These modules self-assemble readily in water and methanol to produce helical RNTs (Fig. S4†) and their respective expression of chirality was monitored by CD (Fig. 2C and D). The point chirality in both modules is very close to the chromophores, resulting in strong CD signals, as observed after one day of self-assembly. In water, R-TBL shows two maxima (39.3 mdeg at 302 nm, 25.8 mdeg at 252 nm) and one minimum (−27.5 mdeg at 236 nm), and S-TBL displays two minima (−32.9 mdeg at 302 nm, −23.2 mdeg at 251 nm) and one maximum (21.2 mdeg at 234 nm). In methanol, two maxima (30.4 mdeg at 286 nm, 24.2 mdeg at 248 nm) and two minima (−29.6 mdeg at 286 nm, −27.0 mdeg at 248 nm) were observed

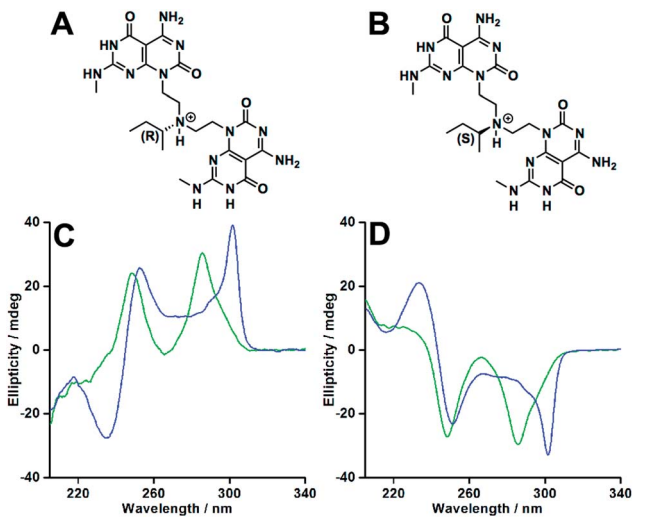

Fig. 2 Twin-G∧C motifs with chiral side-chains at a concentration of 3.34×10^{-5} M: R-TBL (A) and S-TBL (B) and their corresponding CD signals (C and D) in water (blue) and methanol (green) after 1 day of self-assembly.

for R-TBL and S-TBL, respectively. Comparatively, minor differences in the CD profiles were observed in the respective solvents and such differences are known to occur due to the solvent polarity.[37]

3.2 Supramolecular chirality due to solvent and structural differences

Our group has previously reported a solvent-induced supramolecular inversion for RNTs derived from a single-G∧C system in which thermodynamically stable RNTs of opposite helicities were obtained, as evidenced by the mirror-image CD profiles in water and methanol.[38] A new term (chiromer) was introduced, which was used to describe two (or more) conformational states that a molecule can adopt when it forms supramolecular structures. The free energy pathways were found through molecular modeling calculations and it was revealed that the water-chiromer was thermodynamically more favorable in both solvents. However, due to the presence of an initial energy barrier, the formation of the water-chiromer was shown to be kinetically unfavorable and thermodynamically driven, whereas the methanol chiromer was found to be thermodynamically less stable but kinetically favorable as it formed without an energy barrier. It was, however, possible to switch the helicity of the left-handed RNTs (methanol-chiromer) in methanol by either heating the sample or adding a catalytic amount of the right-handed RNTs (water-chiromer) formed in water.

Herein, we were interested in investigating similar behavior for the twin-G∧C system. Our results have shown that R-TBL and S-TBL do not undergo solvent-promoted supramolecular chirality inversion, whereas K-C2-TBL and K-C4-TBL (Fig. 3A and B) behaved differently. While both motifs are functionalized with L-lysine, these building blocks differ in the number of carbon atoms linking the amino acid to the G∧C core (ethyl linker for K-C2-TBL and butyl linker for K-C4-TBL). Both modules self-assembled readily in water and methanol to produce RNTs (Fig. S5†). Similar CD profiles were observed for K-C2-TBL RNTs, with two maxima (14.7 mdeg at 302 nm, 11.1 mdeg at 255 nm) and a minimum (−12.4 mdeg at 240 nm) in water, and two maxima (37.3 mdeg at 302 nm, 26.7 mdeg at 252 nm) and a minimum (−29.7 mdeg at 234 nm) in methanol. However, the intensity of the CD signal in water was lower due to a slower self-assembly rate (Fig. 3C).[27,38]

The CD spectrum for K-C4-TBL RNTs in water was similar to the CD profiles obtained for K-C2-TBL in either solvents, with two maxima (at 302 nm and 254 nm) and a minimum (at 239 nm) (Fig. 3D). Interestingly, a mirror-image CD profile was observed for K-C4-TBL in methanol, with two minima (−84.3 mdeg at 302 nm, −56.4 mdeg at 250 nm) and a maximum (54.5 mdeg at 233 nm). The CD spectra of K-C4-TBL RNTs in water were always mirror-images of the spectra in methanol, thus establishing that the supramolecular chirality recorded was not a random process. A variable temperature CD experiment showed a gradual decrease in ellipticity with

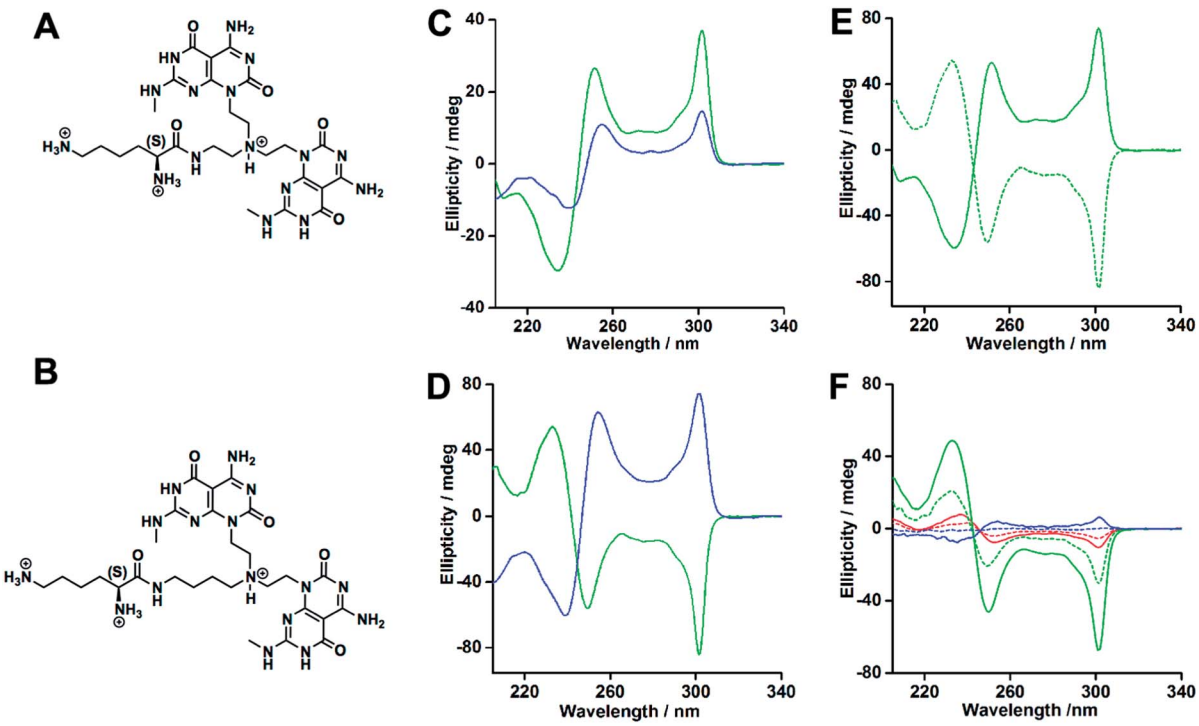

Fig. 3 L-Lysine-functionalized twin-G∧C motifs at a concentration of 2.46×10^{-5} M: K-C2-TBL (A) and K-C4-TBL (B) and their corresponding CD signals (C and D) in water (blue) and methanol (green) after 14 days of self-assembly; and CD signals (E) of K-C2-TBL (solid) and K-C4-TBL (dash) in methanol. For comparison, the spectrum of K-C4-TBL (D) in water was multiplied by a factor of 20 and that of K-C2-TBL (E) in methanol was multiplied by a factor of 2. CD experiments for binary solvent study of K-C4-TBL (F) for non-heated (solid) and heated (dash) samples in methanol (green), water (blue) and 1 : 1 methanol–water mixture (red) after 28 days of self-assembly.

increasing temperature, which was restored upon cooling, thus establishing the supramolecular nature of this chirality (Fig. S6†).

Binary solvent and heat studies were conducted to determine the kinetic *versus* thermodynamic control of the hierarchical self-assembly process. Heat led to a decrease in the intensity of the CD signals for both water and methanol (Fig. 3F), even though the RNTs' population increased upon heating due to a faster rate of self-assembly.[38] Based on our earlier report,[38] we believe that K-C4-TBL self-assembles to produce a kinetic chiromer in water and a thermodynamic chiromer in methanol at ambient temperature, leading to opposite helicities, as expressed by the mirror-image CD signals. We presume that heating the water sample encourages the formation of the thermodynamic chiromer in an otherwise kinetic chiromer-rich environment, leading to a CD-silent spectrum (Fig. 3F, blue-dashed line). Similarly, for the methanolic sample, heating leads to the formation of the kinetic chiromer due to which a depressed CD signal is observed (Fig. 3F, green-dashed line). We did not witness any significant transfer of chirality from the kinetic to the thermodynamic chiromer or *vice versa* from the binary solvent study.

Another interesting observation was that K-C2-TBL and K-C4-TBL displayed opposite helicities in methanol, as reflected by the mirror-image CD profiles (Fig. 3E). K-C2-TBL and K-C4-TBL have the same point chirality and differ only in the length of the side-chain. Evidently, the spatial orientation adopted by the two peptide chains during self-assembly can direct the helicity assumed by the RNTs in solution.

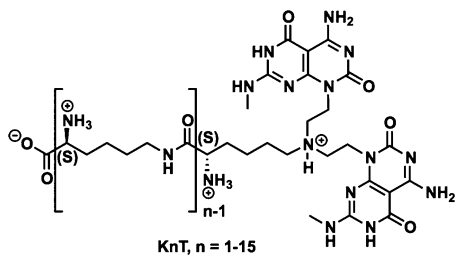

Fig. 4 K1T-K15T:Twin-G∧C compounds functionalized with L-lysine.

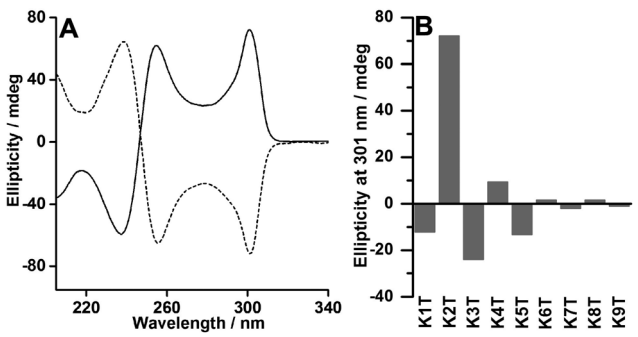

Fig. 5 (A) CD signals of K2T (solid) and K3T (dash) RNTs in unbuffered water. Ellipticity at 301 nm of a 4.0 × 10^{-5} M solution of K1T-K9T in unbuffered water (B). For comparison, the spectrum of K3T in A was multiplied by a factor of 3.

3.3 Supramolecular chirality due to oligomerization of L-lysine

To further investigate the influence of structural changes on the supramolecular chirality of twin-RNTs in methanol, a library of oligo-L-lysine functionalized twin-G∧C modules (K1T-K15T, Fig. 4) was designed.[36] The self-assembly and CD behavior of K3T were investigated in methanol and, unfortunately, a CD-silent spectrum was obtained, which was likely due to limited self-assembly in the organic solvent (Fig. S7†).

The self-assembly and supramolecular chirality of K1T-K15T were also investigated in water. It was found that only modules up to K9T resulted in RNTs in unbuffered water (pH ∼ 4–5). A decrease in the RNTs' length was also observed with increasing number of lysine residues, which is most likely due to the increasing charge density and steric bulk of the growing oligo-lysine chains (Fig. S8†). As observed for K-C4-TBL and K-C2-TBL (Fig. 3E), despite having the same absolute molecular chirality in all K*n*T series, structure-dependent CD spectra were obtained. In fact, a sequential alternating chirality inversion was observed for the motifs, with an odd number (or even) of lysine units having a similar CD signature. For instance, the CD profile for K2T displayed two maxima (72.3 mdeg at 301 nm, 62.0 mdeg at 255 nm) and a minimum (−59.5 mdeg at 273 nm), while K3T showed two minima (−72.3 mdeg at 301 nm, −64.9 mdeg at 256 nm) and a maximum (64.8 mdeg at 239 nm) (Fig. 5A). The decrease in the extent of self-assembly was also reflected by a general lowering of the intensity of the CD signals from K1T to K9T (Fig. 5B).

3.4 Molecular modeling reveals opposite helicities

Molecular modeling calculations[39–41] were performed on K2T–K3T motifs (Fig. S9 and S10†) to determine the orientation of the oligolysine chains on the periphery of the RNTs. The peptide chains in both K2T and K3T motifs engage in inter-rosette hydrogen-bonding interactions, which dictate the ultimate orientation of these chains, hence the resulting supramolecular chirality (Fig. S11†). A preferred helicity was observed for K2T RNTs, which was the opposite of K3T (Fig. 6). It was found that there are hydrogen-bonding interactions between the terminal carboxyl group of an upper rosette and α-amino group of a lower

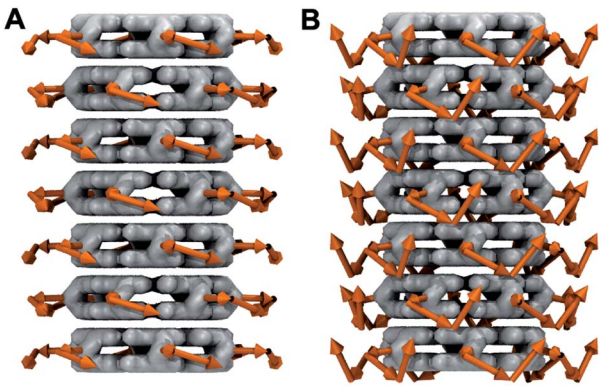

Fig. 6 Molecular models showing the helicity of K2T (A) and K3T (B) RNTs due to the orientation of L-oligolysine chains.

rosette in K2T. As a result, the conformation of the peptide chains on the RNTs is locked, leading to a preferred left-handedness (Fig. 6A). In contrast, K3T has a longer peptidyl chain, and subsequently more possible hydrogen-bonding sites. While inter-rosette hydrogen bonding between the first two lysine residues in the peptide chain locks the conformation in a downward direction, it is the interaction of the terminal carboxyl group that results in a final upward vector (Fig. 6B). Consequently, K3T RNTs adopt a right-handed helicity. As the length of the peptide chain increased, the RNTs self-assembled at a slower rate due to the higher net charge and unfavorable steric interactions. As the oligolysine chains grew longer the dominance of one supramolecular handedness over the other became less pronounced for the same reasons.

3.5 Self-assembly of K10T–K15T at higher pH

As the degree of oligomerization was increased, the rate of self-assembly and formation of RNTs became more challenging. The increase in net surface charge and functional group density led to more pronounced electrostatic steric repulsive forces. In an attempt to neutralize some of the cationic charges on the peptide chains, the self-assembly was investigated at higher pH values. UV-vis spectroscopy was also used to monitor the self-assembly of K9T in unbuffered water and K10T at pH 7 (Fig. 7).

A significant hypochromic effect at $\lambda_{max} = 284$ nm was observed for K9T due to the π–π stacking of double-stacked hexameric rosettes (a 50% change in the absorbance after nine days of self-assembly), which was in agreement with the formation of RNTs (Fig. 7A and B). While no RNTs were produced for K10T at pH 7 after twenty days of self-assembly (Fig. 7C), an increase in basicity (pH 10) led to the formation of long RNTs (Fig. 7E). These results were supported by the absorption spectra obtained for K10T at pH 7 (Fig. 7D) and pH 10 (Fig. 7F), where a higher hypochromic effect was observed at pH 10 due to increased π–π stacking interactions. K11T–K15T also self-assembled to produce RNTs at higher pHs, as confirmed by electron microscopy imaging (Fig. S12 and S13†) and absorption spectra (Fig. S14 and S15†).

3.6 pH controlled chiroptical switching

The supramolecular chirality of K1T–K15T was investigated at higher pHs (pH 7 and pH 11). The sign of the CD profiles for K1T–K3T remained unchanged, irrespective of the pH conditions (unbuffered water, Fig. 5B; pH 7, Fig. S16; pH 11, Fig. S17†). As previously mentioned, K4T–K9T motifs showed a sequential alternating chirality inversion in unbuffered water, however, at pH 7, all modules exhibited the same chirality, with a minimum at 301 nm (Fig. 8). This supramolecular chirality at pH 7 underwent a pH controlled chiroptical switching when the basicity was increased. At pH 11, K4T-K15T self-assembled to produce RNTs and gave the same preferred helicity, which was reflected by a maximum at 301 nm.

Based on these results, we suggest that the observed chiroptical switching is related to the deprotonation of the carboxylic and ammonium groups in the (oligo)lysine moieties. As mentioned earlier, the conformation adopted by the RNT is

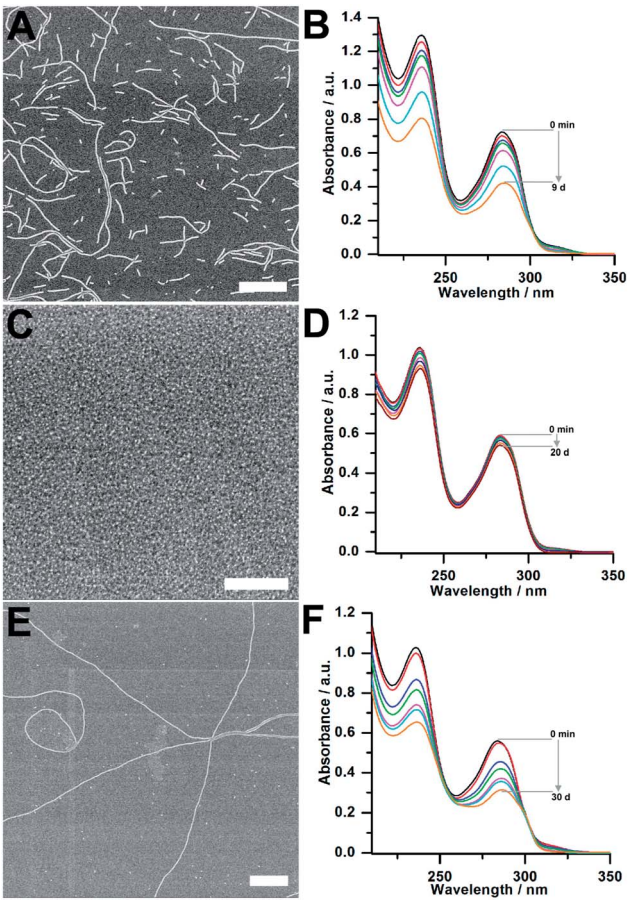

Fig. 7 SEM images and absorption spectra of: K9T in unbuffered water (A and B), K10T at pH 7 (C and D) and K10T at pH 10 (E and F). Scale bar = 300 nm.

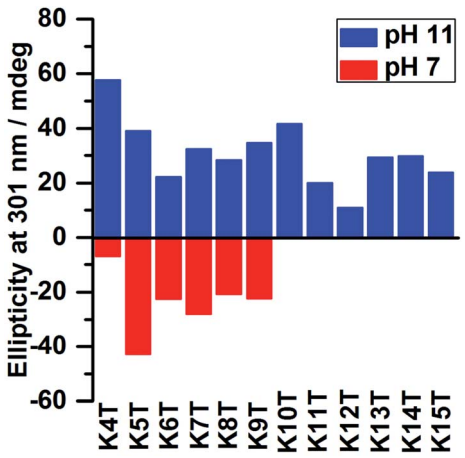

Fig. 8 Ellipticity at 301 nm of a 4.0×10^{-5} M solution of K4T-K15T at pH 7 (red) and pH 11 (blue).

dictated by the inter-rosette hydrogen bonds between the terminal carboxylic acid and ammonium groups of the peptide chains at low pH (unbuffered water). However, due to increased steric interactions resulting from oligomerization, a decrease in chiroptical selectivity was observed. At pH 7, the terminal

carboxylic acid groups in all motifs were unprotonated. In an attempt to reduce the repulsive forces hindering self-assembly, the terminal carboxylate groups in K4T–K9T engage in inter-rosette hydrogen bonding interactions to produce the most stable RNTs. These RNTs have a preferred right-handed helicity. At pH 11, all the ammonium ions were completely neutralized, leading to a significant drop in electrostatic repulsion. Self-assembly at this pH is fastest and RNTs of left-handed helicities were produced for all K4T–K15T motifs. The CD profiles of all RNTs at various pHs are illustrated in Fig. S18 and S19.†

4 Conclusions

In summary, we have described the design, synthesis and characterization of several chiral twin-G∧C motifs. These building blocks undergo a hierarchical self-assembly process under various conditions to produce helical RNTs. The CD experiments revealed interesting chiroptical behavior: (a) RNTs of opposite handedness were obtained due to the presence of *R* or *S* point chirality within the monomers. (b) An example of a solvent-induced supramolecular chirality was also reported resulting from kinetic and thermodynamic self-assembly processes leading to new chiromers.[38] (c) RNTs of opposite helicities were formed despite having the same molecular chirality. The helicity was dictated by the orientation of the side-chain due to inter-rosette hydrogen-bonding interactions, as suggested by molecular modeling. (d) A pH-induced chiroptical switching was also observed for motifs self-assembled at pH 7 and pH 11. At pH 7, the terminal carboxylic acid groups in all motifs exist in the carboxylate, leading to RNTs of right-handed helicity. As the pH was increased to 11, the rate of self-assembly was fastest due to the complete neutralization of the ammonium ions and consequently, RNTs of left-handed helicities were formed preferentially. Such behavior may also be the result of a kinetic *versus* thermodynamic self-assembly process previously identified for a different class of RNTs.[38]

Acknowledgements

We gratefully acknowledge the support from the National Research Council of Canada, the Natural Science and Engineering Research Council of Canada, the University of Alberta, and Northeastern University. U.D.H and M.E.B have equally contributed to this work.

References

1 L. L. Whyte, *Nature*, 1958, **182**, 198.
2 R. S. Cahn, C. Ingold and V. Prelog, *Angew. Chem., Int. Ed.*, 1966, **5**, 385–415.
3 D. B. Amabilino, *Chirality at the Nanoscale*, Wiley-VCH, 2009, pp. 1–217.
4 J.-M. Lehn, *Angew. Chem., Int. Ed.*, 1990, **29**, 1304–1319.
5 M. H. F. Wilkins, R. G. Gosling and W. E. Seeds, *Nature*, 1951, **167**, 759–760.
6 J. D. Watson and F. H. C. Crick, *Nature*, 1953, **171**, 737–738.
7 M. H. F. Wilkins, A. R. Stokes and H. R. Wilson, *Nature*, 1953, **171**, 738–740.
8 R. E. Franklin and R. G. Gosling, *Nature*, 1953, **171**, 740–741.
9 G. D. Fasman, *Circular dichroism and the conformational analysis of biomolecules*, Plenum Press, New York, 1996, pp. 1–738.
10 W. J. Lough and I. W. Wainer, *Chirality in Natural and Applied Science*, CRC Press, Oxford, 2002, pp. 1–313.
11 J.-M. Lehn, *Supramolecular chemistry*, Wiley-VCH, New York, 1995, pp. 1–271.
12 M. Crego-Calama and D. N. Reinhoudt, Supramolecular Chirality, *Top. Curr. Chem.*, 2006, 1–312.
13 S. Vazquez-Campos, M. Crego-Calama and D. N. Reinhoudt, *Supramol. Chem.*, 2007, **19**, 95–106.
14 H. Engelkamp, S. Middelbeek and R. J. M. Nolte, *Science*, 1999, **284**, 785–788.
15 A. P. H. J. Schenning, P. Jonkheijm, E. Peeters and E. W. Meijer, *J. Am. Chem. Soc.*, 2001, **123**, 409–416.
16 C. R. L. P. N. Jeukens, P. Jonkheijm, F. J. P. Wijnen, J. C. Gielen, P. C. M. Christianen, A. P. H. J. Schenning, E. W. Meijer and J. C. Maan, *J. Am. Chem. Soc.*, 2005, **127**, 8280–8281.
17 M. M. Green, N. C. Peterson, T. Sato, A. Teramoto, R. Cook and S. Lifson, *Science*, 1995, **268**, 1860–1866.
18 M. M. Green, M. P. Rediy, R. J. Johnson, G. Darling, D. J. O'leary and G. Willson, *J. Am. Chem. Soc.*, 1989, **111**, 6452–6454.
19 A. R. A. Palmans, J. A. J. M. Vekemans, E. E. Havinga and E. W. Meijer, *Angew. Chem., Int. Ed.*, 1997, **36**, 2648–2651.
20 L. Brunsveld, E. W. Meijer, R. B. Prince and J. S. Moore, *J. Am. Chem. Soc.*, 2001, **123**, 7978–7984.
21 L. Brunsveld, J. A. J. M. Vekemans, J. H. K. K. Hirschberg, R. P. Sijbesma and E. W. Meijer, *Proc. Natl. Acad. Sci. U. S. A.*, 2002, **99**, 4977–4982.
22 K. Nakanishi, N. Berova and R. W. Woody, *Circular Dichroism Principles and Applications*, Wiley-VCH, New York, 1994, pp. 1–230.
23 E. Yashima, K. Maeda and Y. Okamoto, *Science*, 1999, **399**, 449–451.
24 G. M. Whitesides, J. P. Mathias and C. T. Seto, *Science*, 1991, **254**, 1312–1319.
25 L. J. Prins, F. De Jong, P. Timmerman and D. N. Reinhoudt, *Nature*, 2000, **408**, 181–184.
26 J. Huskens, F. De Jong, P. Timmerman and D. N. Reinhoudt, *Nature*, 1999, **398**, 498–502.
27 H. Fenniri, B. L. Deng and A. E. Ribbe, *J. Am. Chem. Soc.*, 2002, **124**, 11064–11072.
28 H. Fenniri, P. Mathivanan, K. L. Vidale, D. M. Sherman, K. Hallenga and K. V. Wood, *J. Am. Chem. Soc.*, 2001, **123**, 3854–3855.
29 H. Fenniri, B. L. Deng, A. E. Ribbe, K. Hallenga, J. Jacob and P. Thiyagarajan, *Proc. Natl. Acad. Sci. U. S. A.*, 2002, **99**, 6487–6492.
30 J. G. Moralez, J. Raez, T. Yamazaki, M. R. Kishan, A. Kovalenko and H. Fenniri, *J. Am. Chem. Soc.*, 2005, **127**, 8307–8309.

31 L. Zhang, U. D. Hemraz, H. Fenniri and T. J. Webster, *J. Biomed. Mater. Res., Part A*, 2010, **95**, 550–563.
32 L. Sun, L. Zhang, U. D. Hemraz, H. Fenniri and T. J. Webster, *Tissue Eng., Part A*, 2012, **18**, 1741–1750.
33 A. Childs, U. D. Hemraz, N. J. Castro, H. Fenniri and L. G. Zhang, *J. Biomed. Mater. Res. A*, 2013, **8**, 065003.
34 G. Borzsonyi, R. S. Johnson, A. J. Myles, J. Y. Cho, T. Yamazaki, R. L. Beingessner, A. Kovalenko and H. Fenniri, *Chem. Commun.*, 2010, **46**, 6527–6529.
35 G. Borzsonyi, R. L. Beingessner, T. Yamazaki, J. Y. Cho, A. J. Myles, M. Malac, R. Egerton, M. Kawasaki, K. Ishizuka, A. Kovalenko and H. Fenniri, *J. Am. Chem. Soc.*, 2010, **132**, 15136–15139.
36 Manuscript in preparation.
37 A. Avdagić, A. Lesac and V. Šunjić, *Tetrahedron*, 1999, **55**, 1407–1416.
38 R. S. Johnson, T. Yamazaki, A. Kovalenko and H. Fenniri, *J. Am. Chem. Soc.*, 2007, **129**, 5735–5743.
39 A. Kovalenko and F. Hirata, *J. Chem. Phys.*, 1999, **110**, 10095–10112.
40 A. Kovalenko and F. Hirata, *J. Chem. Phys.*, 2000, **112**, 10391–10417.
41 T. Yamazaki, H. Fenniri and A. Kovalenko, Chiromerism: Conformation-dependent supramolecular chirality, *ChemPhysChem*, 2010, **11**, 361–367.